Square lattice photonic crystal point-shifted nanocavity with lowest-order whispering-gallery mode

Tsan-Wen Lu,* Pin-Tso Lin, Kuan-Un Sio, and Po-Tsung Lee

Department of Photonics and Institute of Electro-Optical Engineering, National Chiao Tung University, Rm. 415 CPT Building, 1001 Ta Hsueh Road, Hsinchu 300, Taiwan
**ricky.eo94g@nctu.edu.tw*

Abstract: We propose a point-shifted nanocavity based on square lattice photonic crystal, which sustains a lowest-order whispering-gallery (WG) mode. In simulation, the optimized WG mode (quality (Q) factor ~14,000) in point-shifted nanocavity can be with smaller mode volume (~$5.5(\lambda/2n)^3$) but larger nano-post tolerance than those in single-defect cavity design. From well-fabricated device, single WG mode lasing with measured Q factor of 4,100 and low threshold of 160 μW is obtained. Besides, we also observe the changed polarization of WG mode due to modal symmetry breaking caused by the presence of a nearby dielectric nano-particle, which would be useful in sensing molecule binding or attaching for bio-chemical applications.

OCIS codes: (230.5298) Photonic crystals; (140.3945) Nanocavities; (140.5960) Semiconductor lasers.

References and links

1. O. Painter, R. K. Lee, A. Scherer, A. Yariv, J. D. O'Brien, P. D. Dapkus, and I. Kim I, "Two-dimensional photonic band-Gap defect mode laser," Science **284**(5421), 1819–1821 (1999).
2. H. Hagino, Y. Takahashi, Y. Tanaka, T. Asano, and S. Noda, "Effects of fluctuation in air hole radii and positions on optical characteristics in photonic crystal heterostructure nanocavities," Phys. Rev. B **79**(8), 085112 (2009).
3. M. Notomi, and H. Taniyama, "On-demand ultrahigh-Q cavity formation and photon pinning via dynamic waveguide tuning," Opt. Express **16**(23), 18657–18666 (2008).
4. M. Notomi, E. Kuramochi, and H. Taniyama, "Ultrahigh-Q nanocavity with 1D photonic gap," Opt. Express **16**(15), 11095–11102 (2008).
5. H. S. Ee, K. Y. Jeong, M. K. Seo, Y. H. Lee, and H. G. Park, "Ultrasmall square-lattice zero-cell photonic crystal laser," Appl. Phys. Lett. **93**(1), 011104 (2008).
6. T. Yamamoto, M. Notomi, H. Taniyama, E. Kuramochi, Y. Yoshikawa, Y. Torii, and T. Kuga, "Design of a high-Q air-slot cavity based on a width-modulated line-defect in a photonic crystal slab," Opt. Express **16**(18), 13809–13817 (2008).
7. K. Nozaki, S. Kita, and T. Baba, "Room temperature continuous wave operation and controlled spontaneous emission in ultrasmall photonic crystal nanolaser," Opt. Express **15**(12), 7506–7514 (2007).
8. J. Chan, M. Eichenfield, R. Camacho, and O. Painter, "Optical and mechanical design of a "zipper" photonic crystal optomechanical cavity," Opt. Express **17**(5), 3802–3817 (2009).
9. T. Yoshie, A. Scherer, J. Hendrickson, G. Khitrova, H. M. Gibbs, G. Rupper, C. Ell, O. B. Shchekin, and D. G. Deppe, "Vacuum Rabi splitting with a single quantum dot in a photonic crystal nanocavity," Nature **432**(7014), 200–203 (2004).
10. M. Eichenfield, R. Camacho, J. Chan, K. J. Vahala, and O. Painter, "A picogram- and nanometre-scale photonic-crystal optomechanical cavity," Nature **459**(7246), 550–555 (2009).
11. A. Di Falco, L. O'Faolain, and T. F. Krauss, "Chemical sensing in slotted photonic crystal heterostructure cavities," Appl. Phys. Lett. **94**(6), 063503 (2009).
12. S. H. Kwon, T. Sünner, M. Kamp, and A. Forchel, "Optimization of photonic crystal cavity for chemical sensing," Opt. Express **16**(16), 11709–11717 (2008).
13. S. Kita, K. Nozaki, and T. Baba, "Refractive index sensing utilizing a cw photonic crystal nanolaser and its array configuration," Opt. Express **16**(11), 8174–8180 (2008).
14. K. Nozaki, H. Watanabe, and T. Baba, "Photonic crystal nanolaser monolithically integrated with passive waveguide for effective light extraction," Appl. Phys. Lett. **92**(2), 021108 (2008).

#120574 - $15.00 USD Received 30 Nov 2009; revised 15 Jan 2010; accepted 17 Jan 2010; published 22 Jan 2010

15. Y. Takahashi, Y. Tanaka, H. Hagino, T. Sugiya, Y. Sato, T. Asano, and S. Noda, "Design and demonstration of high-*Q* photonic heterostructure nanocavities suitable for integration," Opt. Express **17**(20), 18093–18102 (2009).
16. S. Chakravarty, P. Bhattacharya, and Z. Mi, "Electrically Injected Quantum-Dot Photonic Crystal Microcavity Light-Emitting Arrays With Air-Bridge Contacts," IEEE Photon. Technol. Lett. **18**(24), 2665–2667 (2006).
17. T. W. Lu, P. T. Lee, C. C. Tseng, and Y. Y. Tsai, "Modal properties and thermal behaviors of high quality factor quasi-photonic crystal microcavity," Opt. Express **16**(17), 12591–12598 (2008).
18. Y. K. Kim, V. C. Elarde, C. M. Long, J. J. Coleman, and K. D. Choquette, "Electrically injected InGaAs/GaAs photonic crystal membrane light emitting microcavity with spatially localized gain," J. Appl. Phys. **104**(12), 123103 (2008).
19. W. D. Ho, T. W. Lu, Y. H. Hsiao, and P. T. Lee, "Thermal Properties of 12-Fold Quasi-Photonic Crystal Microcavity Laser with Size-Controlled Nano-Post for Electrical Driving," J. Lightwave Technol. **27**(23), 5302–5307 (2009).
20. H. G. Park, S. H. Kim, S. H. Kwon, Y. G. Ju, J. K. Yang, J. H. Baek, S. B. Kim, and Y. H. Lee, "Electrically driven single-cell photonic crystal laser," Science **305**(5689), 1444–1447 (2004).
21. M. K. Seo, K. Y. Jeong, J. K. Yang, Y. H. Lee, H. G. Park, and S. B. Kim, "Low threshold current single-cell hexapole mode photonic crystal laser," Appl. Phys. Lett. **90**(17), 171122 (2007).
22. H. Y. Ryu, J. K. Hwang, and Y. H. Lee, "The smallest possible whispering-gallery-like mode in the square lattice photonic-crystal slab single-defect cavity," IEEE J. Quantum Electron. **39**(2), 314–322 (2003).
23. H. Altug, and J. Vucković, "Photonic crystal nanocavity array laser," Opt. Express **13**(22), 8819–8828 (2005).
24. J. H. Kang, M. K. Seo, S. K. Kim, S. H. Kim, M. K. Kim, H. G. Park, K. S. Kim, and Y. H. Lee, "Polarized vertical beaming of an engineered hexapole mode laser," Opt. Express **17**(8), 6074–6081 (2009).
25. M. R. Lee, and P. M. Fauchet, "Nanoscale microcavity sensor for single particle detection," Opt. Lett. **32**(22), 3284–3286 (2007).
26. A. M. Armani, R. P. Kulkarni, S. E. Fraser, R. C. Flagan, and K. J. Vahala, "Label-free, single-molecule detection with optical microcavities," Science **317**(5839), 783–787 (2007).
27. F. Vollmer, and S. Arnold, "Whispering-gallery-mode biosensing: label-free detection down to single molecules," Nat. Methods **5**(7), 591–596 (2008).

1. Introduction

Since the first demonstration [1], photonic crystal (PhC) micro- and nano-cavities have shown the abilities of strongly controlling photons in a wavelength-scale resonator with very low optical losses [2–4]. In recent years, various one- (1D) and two-dimensional (2D) PhC nanocavities with ultra-small mode volumes close to half-wavelength cubic and high quality (Q) factors have been proposed and demonstrated [5–8]. These PhC nanocavities with energy concentration in one- or half-wavelength cubic volume are very beneficial for enhancing interactions between light and matters in quantum-electro-dynamic phenomenon studies [9], opto-mechanical researches [8,10], optical sensing applications [11–13], and so on. In addition, this kind of ultra-small nanocavity is also promising in achieving thresholdless nanolasers which can be integrated on photonic integrated chip (PIC) [14,15]. Electrical excitation is very important for such nano-laser sources embedded in PIC. However, most nanolaser mode candidates reported are monopole or confined waveguide Bloch modes, which lack of proper current injection approaches. Recently, the strong potential of whispering-gallery (WG) mode in achieving electrically-driven PhC nanolaser sources have been widely investigated [16–19] and successfully demonstrated by inserting a nano-post beneath the cavity [20,21]. The nano-post plays the roles of efficient current pathway and heat sink at the same time without disturbing WG mode due to its central field node. In this report, we propose a point-shifted nanocavity which can sustain a lowest-order WG mode based on square-PhCs. Although the lowest-order WG mode also exists in square-PhC single-defect (D_1) nanocavity [22,23], we show the WG mode in our proposed design here can be with smaller mode volume but larger nano-post tolerance than that in square-PhC D_1 nanocavity.

#120574 - $15.00 USD Received 30 Nov 2009; revised 15 Jan 2010; accepted 17 Jan 2010; published 22 Jan 2010

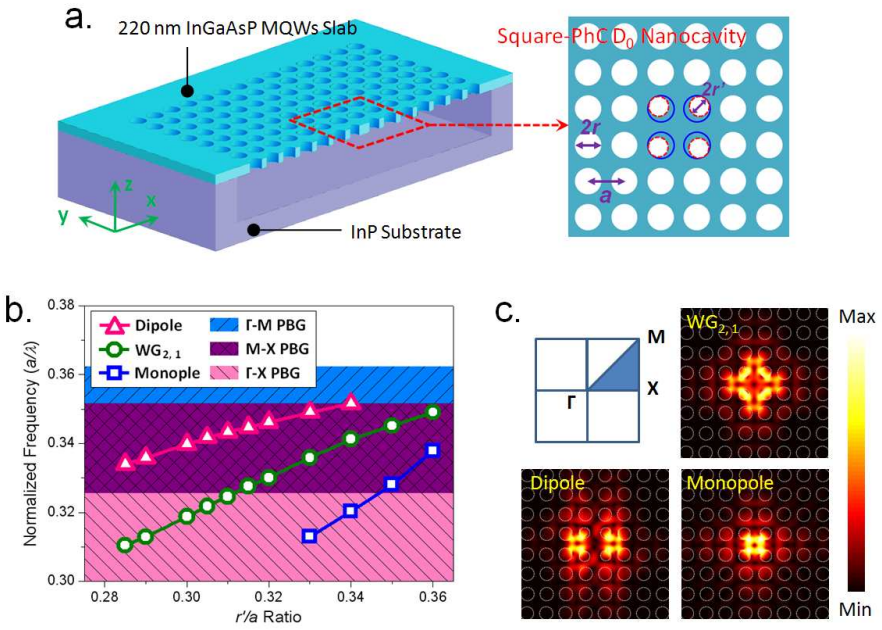

Fig. 1. (a) Scheme of square-PhC D_0 nanocavity on a suspended dielectric slab. (b) The plot of FDTD simulated defect modes frequency versus r'/a ratio in square-PhC D_0 nanocavity under fixed r/a ratio = 0.38, including dipole (open triangle), $WG_{2,1}$ (open circle), and monopole (open square) modes. Γ-M (blue shadow) direction PBG, Γ-X (pink shadow) direction PBG, and their overlapped region M-X direction PBG (purple shadow) are also shown. (c) FDTD simulated mode profiles in electric field of dipole, $WG_{2,1}$, and monopole modes, which are obtained under r'/a ratios of 0.30, 0.30, and 0.35, respectively.

2. Nanocavity design and simulations

Generally, square-PhC has smaller photonic band gap (PBG) comparing with triangular one. To make sure that the defect modes will be well-confined by the PBG effect, we calculate the band diagram of square-PhC dielectric slab by three-dimensional (3D) plane wave expansion method. The slab thickness and refractive index are set to be 220 nm and 3.4, respectively. The structure scheme is shown in Fig. 1(a). The simulated results indicate that the PBG width increases with r/a ratio, where r and a represent air-hole radius and lattice constant, respectively. For example, the PBG region is ranged from 0.326 to 0.352 in normalized frequency (a/λ) under r/a ratio = 0.38, which corresponds to a sufficient large spectral width of 110 nm when a = 500 nm. Although wider PBG range can be obtained when r/a ratio is larger than 0.38, the PhC structure becomes fragile in fabrication due to the enlarged air-hole radius. Thus, the r/a ratio of square-PhC will be chosen and fixed to be 0.38 from now on.

A simple square-PhC nanocavity design is the D_1 nanocavity by removing an air-hole and a lowest-order $WG_{2,1}$ (the former and latter sub-number represent the azimuthal number and radial order, respectively) mode will be sustained in this nanocavity design [22,23]. Recently, it has been reported that local lattice shifts in 1D or 2D PhCs can create nanocavities well sustaining various ultra-small defect modes [5–8]. In this report, we propose a nanocavity design using similar approach based on square-PhCs. As shown in Fig. 1(a), the square PhCs are defined by air holes on a suspended dielectric slab. Four central air holes are shrunk to be r' in radius and the positions are shifted outward to form a nanocavity region, named point-shifted D_0 nanocavity.

First, we perform 3D finite-difference time-domain (FDTD) simulations to obtain the defect modes in this nanocavity design. In the simulation setup, the lattice constant, r/a ratio, slab thickness, and refractive index are set to be 500 nm, 0.38, 220 nm, and 3.4, respectively. The r'/a ratio is varied from 0.285 to 0.36, and the number of lattice periods is set to be 14 in

#120574 - $15.00 USD Received 30 Nov 2009; revised 15 Jan 2010; accepted 17 Jan 2010; published 22 Jan 2010

both *x*- and *y*-directions to provide sufficient PBG confinement. From the simulation results, three defect modes exist in D_0 nanocavity under different *r'/a* ratios, including dipole, $WG_{2,1}$, and monopole modes. The relationship between the simulated defect mode frequency and *r'/a* ratio of square-PhC D_0 nanocavity are shown in Fig. 1(b). All the defect modes lie inside the PBG region. As shown in Fig. 1(b), we also find that $WG_{2,1}$ and monopole modes can be confined only by *Γ-X* direction PBG effect. This is possible because the in-plane radiations of $WG_{2,1}$ and monopole modes are mainly along *Γ-X* direction, which can be observed from the FDTD simulated mode profiles in electrical field shown in Fig. 1(c). Thus, for both $WG_{2,1}$ and monopole modes, the available design range will be larger than the expected *M-X* direction PBG region. It should be noted that $WG_{2,1}$ mode in D_0 nanocavity is different from $WG_{2,1}$ mode in D_1 nanocavity with in-plane radiation along *Γ-M* direction.

As mentioned before, due to the potential of WG mode in electrically-driven nanolaser based on nano-post structure, we only focus on $WG_{2,1}$ mode in the proposed D_0 nanocavity here. To optimize $WG_{2,1}$ modal properties, we calculate *Q* factor and mode volume variations of $WG_{2,1}$ mode under different *r'/a* ratios. As shown in Fig. 2(a), the maximum *Q* ~14,000 and minimum mode volume ~$5.5(\lambda/2n)^3$ (~0.065 μm^3) are obtained both when *r'/a* = 0.30. It should be noted that the $WG_{2,1}$ mode volume in this D_0 nanocavity design is even smaller than that in square-PhC D_1 nanocavity (~$6.5(\lambda/2n)^3$, ~0.078 μm^3) under the same simulation setup. And the calculated Purcell factor of $WG_{2,1}$ mode under this *r'/a* ratio is around 1,500.

Then we further investigate the tolerance of $WG_{2,1}$ mode when inserting a nano-post beneath the D_0 nanocavity for the electrical-driving purpose, as shown in the inset of Fig. 2(b). The PhC lattice parameters are chosen as *r'/a* = 0.30 and *r/a* = 0.38 according to optimization results. The simulated *Q* factors of $WG_{2,1}$ mode under different nano-post sizes are shown in Fig. 2(b). Obviously, there is significant degradation in *Q* factor when the nano-post size is larger than 0.6*a* in diameter, where the *Q* factor is still larger than 10,000. The extra leaky components inside the light cone induced by the nano-post are responsible for the *Q* degradation [17]. Comparing with $WG_{2,1}$ mode in square-PhC D_1 nanocavity, the *Q* factor degrades significantly when the nano-post size is larger than 0.4*a* in diameter. When nano-post size increases to 0.6*a*, the *Q* factor decreases to be smaller than 5,000. This directly indicates the larger nano-post tolerance of $WG_{2,1}$ mode in D_0 nanocavity proposed here than in single-defect one. In addition, we also show the simulated *Q* factor variations of dipole and monopole modes in D_0 nanocavity with different nano-post sizes for comparison. The *r'/a* ratios are chosen as 0.30 and 0.35 for dipole and monopole modes, which correspond to their highest *Q* factors of 2,200 and 11,000, respectively. For monopole mode, although the high *Q* factor indicates that it will be one of the dominant modes in this nanocavity, its *Q* factor

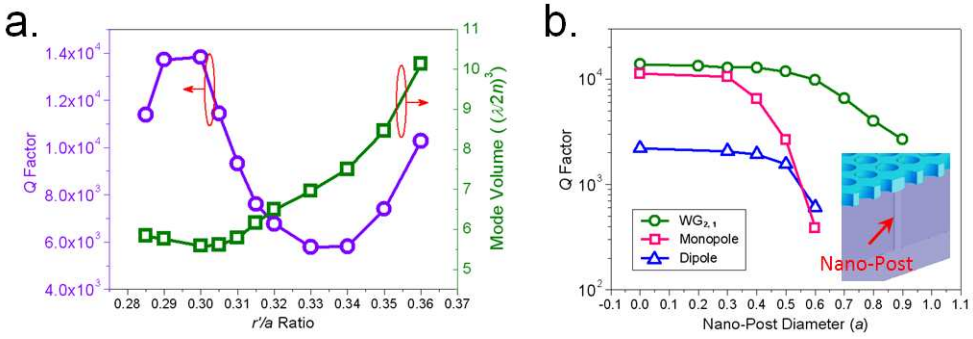

Fig. 2. (a) The simulated *Q* factor (open circles) and mode volume (open squares) of $WG_{2,1}$ mode in D_0 nanocavity under different *r'/a* ratios. The highest *Q* factor and smallest mode volume are both obtained when *r'/a* = 0.30. (b) Scheme of square-PhC D_0 nanocavity with a nano-post beneath and the simulated *Q* factors of $WG_{2,1}$ (open circle), monopole (open square), and dipole (open triangle) modes in square-PhC D_0 nanocavity with different nano-post diameters.

#120574 - $15.00 USD Received 30 Nov 2009; revised 15 Jan 2010; accepted 17 Jan 2010; published 22 Jan 2010

significantly degrades when the nano-post size is larger than 0.3*a* in diameter. This small nano-post tolerance may increase the difficulty in fabricating this delicate nano-post (150 nm in diameter only). On the other hand, we observe large nano-post tolerance of 0.5*a* from dipole mode. However, due to its low *Q* factor close to 1,000, it will not be the mode candidate for lasing action in D_0 nanocavity. Besides, from Fig. 2(b), we can see the *Q* factors of dipole and monopole modes will both degrade to be smaller than 600 when the nano-post size is 0.6*a* in diameter.

From above simulation results, we can conclude that $WG_{2,1}$ mode in D_0 nanocavity design proposed here has smaller mode volume and larger tolerance when inserting a nano-post beneath than that in D_1 nanocavity. This large nano-post tolerance hosts advantages in electrically-driven structure based on nano-post, including fabrication tolerance, low electrical resistance, improved heat sink, and so on [19,20].

3. Characterization of fabricated devices

Real devices are fabricated on InGaAsP multi-quantum-wells (MQWs) by electron-beam lithography and a series of inductively coupled plasma / reactive ion etching dry-etching process. Then the suspended slab is formed by HCl selective wet-etching process [17,19]. Top-, zoom-in, and tilted-view scanning electron microscope (SEM) pictures of fabricated square-PhC D_0 nanocavity are shown in Fig. 3. The fabricated square-PhC D_0 nanocavities are optically pumped at room temperature. To avoid thermal problems, the duty cycle and width of optical pulse are set to be 0.2% and 40 ns, respectively. And the pump spot size is focused to be around 3.5 μm in diameter. From nanocavity with fabricated a = 500 nm, r/a ~0.38, and r'/a = 0.30, we obtain single-mode lasing at 1560 nm, which can be identified as $WG_{2,1}$ mode by comparing with the simulation results in Fig. 1(b). The measured light-in light-out (*L-L*) curve and spectrum of single-mode lasing action are shown in Fig. 4(a) and (b). The threshold is estimated to be 160 μW from the *L-L* curve, which corresponds to an effective threshold as low as 8 μW when taking the power absorbed by the nanocavity into account only. This low threshold is attributed to the small mode volume and high *Q* factor of $WG_{2,1}$ mode in D_0 nanocavity, which directly indicates the potential in achieving thresholdless nanolaser. We also obtain the spectrum below threshold (at 100 μW, ~0.7 times threshold), as shown in the inset of Fig. 4(a). The estimated spectral line-width by Lorentzian fitting is 0.38 nm, which corresponds to a *Q* factor of 4,100. And the measured side-mode suppression-ratio (SMSR) is larger than 20 dB as shown in the inset spectrum of Fig. 4(b).

Besides, from a fabricated square-PhC D_0 nanocavity array with increased r'/a ratio from 0.285 to 0.315 and fixed r/a ratio, we obtain a gradual wavelength shift that matches with the simulation results, as shown in Fig. 4(c). This gradual wavelength shift also directly indicates the lasing action comes from localized cavity mode instead of extended band-edge mode.

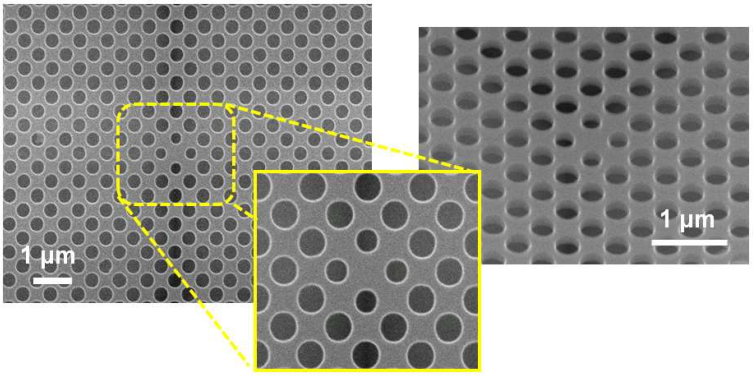

Fig. 3. Top-, zoom-in, and tilted-view SEM pictures of fabricated square-PhC D_0 nanocavity from left to right. The fabricated lattice constant, r/a, and r'/a ratios are 500 nm, 0.38, and 0.30, respectively.

#120574 - $15.00 USD Received 30 Nov 2009; revised 15 Jan 2010; accepted 17 Jan 2010; published 22 Jan 2010

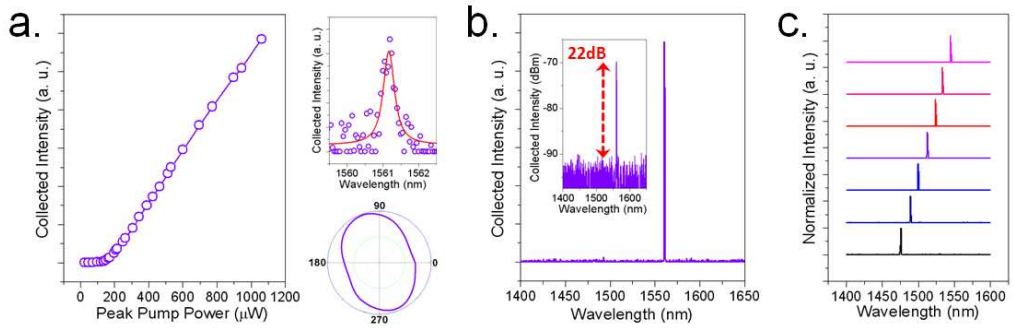

Fig. 4. (a) The measured *L-L* curve and (b) lasing spectrum of $WG_{2,1}$ mode at wavelength of 1560 nm from square-PhC D_0 nanocavity. The measured WG mode polarization and spectrum below threshold are shown in the insets of (a). The lasing spectrum in logarithm scale is shown in the inset of (b). The *r/a* ratio, *r'/a* ratio, and lattice constant of the measured device are 0.38, 0.30, and 500 nm, respectively. (c) $WG_{2,1}$ mode lasing spectra from square-PhC D_0 nanocavities with increased *r'/a* ratio from 0.285 (top curve) to 0.315 (bottom curve) under lattice constant of 480 nm. The intensity of each spectrum has been normalized.

We also measure the polarization of lasing mode by a linear polarizer as shown in the inset of Fig. 4(a), which shows very low polarized degree of 0.21, where the polarized degree is defined as $(I_{max}-I_{min}) / (I_{max} + I_{min})$. This $WG_{2,1}$ modal symmetry with low-polarized property is caused by the equal contributions of electric fields in *x*- and *y*-directions (E_x and E_y) of $WG_{2,1}$ mode in this square-PhC D_0 nanocavity with C_{4v} symmetry, which is a feature of WG mode and could also be an evidence of $WG_{2,1}$ mode lasing. Most importantly, this low polarized degree also indicates that our fabrication uniformity can promise the well balanced four nearest air holes [17,21] of the square-PhC D_0 nanocavity, which leads to $WG_{2,1}$ modal symmetry due to the equal distributions of E_x and E_y components.

In reality, this modal symmetry can be broken by deliberate designs or fabrication non-uniformities and the WG mode will become polarized. In our devices, we observe this modal symmetry breaking due to local disturbance. For example, a dielectric nano-particle existing nearby the nanocavity can affect E_x and E_y components separately. This may result in a dominated electric field component in specific direction and the $WG_{2,1}$ mode will become polarized. In experiments, we compare the $WG_{2,1}$ mode lasing actions from square-PhC D_0 nanocavities with and without a 350 nm-diameter dielectric nano-particle nearby, as shown in the SEM pictures in Fig. 5(a). These two nanocavities are fabricated on the same wafer by the same process and there are only very slight differences in *r/a* and *r'/a* ratios between these two nanocavities. For each nanocavity, the *r/a* and *r'/a* ratios are very uniform. From measured polarizations shown in Fig. 5(b), the polarized degree of $WG_{2,1}$ mode increases to be 0.69, that is, the $WG_{2,1}$ mode becomes polarized, when the nano-particle is introduced nearby the nanocavity. This significant change in polarization could be attributed to the comparable size of the D_0 nanocavity and the nano-particle. To confirm this polarization variation comes from the nano-particle instead of the fabrication non-uniformity of the inner air holes, we measure other nanocavities on the same wafer. We find almost all the nanocavities without nano-particles show very low-polarized property, which indicates the $WG_{2,1}$ mode in fabricated square-PhC D_0 nanocavities suffers very small fabrication imperfections. On the other hand, most nanocavities with nano-particles show high-polarized property. The polarization depends on the direction and distance of nano-particle to the nanocavity. The measured *L-L* curves of these two cases are also shown in Fig. 5(c). The slope efficiency increases significantly when the nano-particle is presented. This is because when the nano-particle breaks the modal symmetry of $WG_{2,1}$ mode, it also breaks the $WG_{2,1}$ modal cancellation in the far field. As a result, there will be more radiation components collected [24] by the objective lens and lead to the increased slope efficiency.

#120574 - $15.00 USD Received 30 Nov 2009; revised 15 Jan 2010; accepted 17 Jan 2010; published 22 Jan 2010

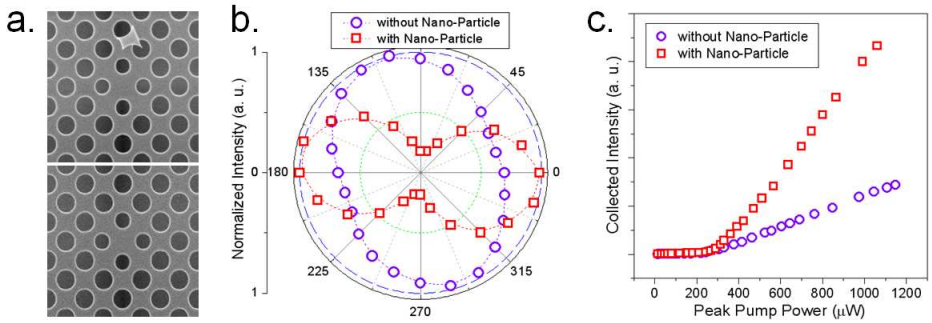

Fig. 5. (a) Top-view SEM pictures of square-PhC D_0 nanocavities (top) with and (bottom) without a 350 nm nano-particle nearby. The measured (b) polarizations and (c) *L-L* curves of $WG_{2,1}$ mode in square-PhC D_0 nanocavities with (open square) and without (open circle) a nano-particle nearby.

We think this observed unique behavior of $WG_{2,1}$ mode in D_0 nanocavity could be used to detect nano-particles based on the polarization variation, which is a spectral-free approach. That means the requirement of very high Q factors in PhC nanocavities by very delicate modulations is not essential for detection down to single molecule binding or attaching via this approach. Thus, we believe this polarization sensing approach would be potential in optically sensing single molecule binding or attaching [25–27] in bio-chemical or drug discovery researches by further investigations.

4. Summary

In this report, we propose a square-PhC D_0 nanocavity formed by shifting and shrinking the four nearest air holes, which can well sustain a lowest-order $WG_{2,1}$ mode. From 3D FDTD simulations, we obtain smaller $WG_{2,1}$ mode volume (~$5.5(\lambda/2n)^3$) and larger nano-post tolerance (~$0.6a$) than those in square-PhC D_1 nanocavity, which is very potential in achieving electrically-driven thresholdless nanolaser based on nano-post structure. From the well-fabricated devices, we obtain and identify single $WG_{2,1}$ mode lasing at 1560 nm with low threshold of 160 μW, measured Q factor of 4,100, and SMSR larger than 20 dB. We also observe $WG_{2,1}$ modal symmetry breaking due to a 350 nm dielectric nano-particle nearby the D_0 nanocavity in experiments, that is, the un-polarized $WG_{2,1}$ mode will become polarized. This polarization variation could be used as a spectral-free approach to sense single molecule binding and attaching in bio-chemical or drug discovery researches, where very high Q factor is not required.

Acknowledgements

This work is supported by Taiwan's National Science Council (NSC) under contract numbers NSC-98-2120-M-009-002 and NSC-98-2221-E-009-015-MY2. The authors would like to thank the help from Center for Nano Science and Technology (CNST) of National Chiao Tung University, Taiwan.

#120574 - $15.00 USD Received 30 Nov 2009; revised 15 Jan 2010; accepted 17 Jan 2010; published 22 Jan 2010